The Astrophysical Journal, 629:328–333, 2005 August 10

THE DISCOVERY OF THE OPTICAL AND NEAR-IR AFTERGLOWS OF THE FIRST *SWIFT* GAMMA-RAY BURSTS

E. Berger,[1,2,3] D. B. Fox,[4] S. R. Kulkarni,[4] W. Krzeminski,[5] A. M. Soderberg,[4] D. A. Frail,[6] D. N. Burrows,[7] S. B. Cenko,[4] E. J. Murphy,[8] P. A. Price,[9] A. Gal-Yam,[3,4] D.-S. Moon,[4] N. Gehrels,[10] W. L. Freedman,[1] S. E. Persson,[1] S. Barthelmy,[10] J. E. Hill,[7] J. A. Nousek,[7] and A. Moretti[11]

Received 2005 February 22; accepted 2005 April 25

ABSTRACT

We present optical and near-infrared searches for afterglow emission from the first four *Swift* bursts with accurate positions from the X-Ray Telescope (XRT). Using telescopes at Las Campanas, Keck, and Palomar observatories, we rapidly identified and followed up afterglows for three of the four bursts and subsequently identified the redshift of GRB 050126 ($z = 1.290$). In three cases the burst positions were also observed with the Very Large Array, but no radio afterglow emission was detected. The optical/near-IR afterglows are fainter than about 70% of all afterglows detected to date, with GRB 050126 being the faintest, and were identified thanks to accurate and rapid positions from the XRT and rapid response with $\gtrsim 1$ m telescopes. This suggests that the fraction of dust-obscured bursts is small, $\lesssim 20\%$ when combined with afterglows localized by the *HETE-2* Soft X-ray Camera. The X-ray fluxes are typical of the known population, with the exception of GRB 050126, which has the faintest X-ray afterglow to date (normalized to $\Delta t = 10$ hr) and was detected thanks to a response time of only 130 s after the burst. Finally, we find that all three optical/near-IR afterglows are located $\lesssim 2''$ away from the nominal XRT positions, suggesting that the XRT is capable of delivering highly accurate positions, which will revolutionize afterglow studies.

Subject heading: gamma rays: bursts

1. INTRODUCTION

The *Swift* gamma-ray satellite (Gehrels et al. 2004), launched on 2004, November 20, holds great promise for our understanding of gamma-ray bursts (GRBs), as well as their use for cosmological applications. This is primarily because of the positional accuracy and great sensitivity of the Burst Alert Telescope (BAT) and the on-board X-Ray Telescope (XRT) and UV/Optical Telescope (UVOT), which are capable of providing $\sim 0\farcs3$–$5''$ positions and detailed light curves within a few minutes after the burst. Starting in mid-December 2004 *Swift* has localized several bursts, of which a few have been followed up with the XRT, providing $\sim 8''$–$30''$ error circles on a timescale of several hours. The rapidity and accuracy of these localizations have enabled deep ground-based optical and near-infrared (NIR) searches.

Here we present a comprehensive investigation (optical, NIR, radio) of the first four *Swift* bursts with XRT detections: GRBs 041223, 050117a, 050124, and 050126. The observations were conducted at Las Campanas Observatory (LCO), Palomar Observatory, Keck Observatory, and the Very Large Array (VLA). Even at this early stage, with the localization timescale and accuracy still an order of magnitude below the eventual capability of *Swift*, the combination of *Swift* and $\gtrsim 1$ m class ground-based telescopes suggests that the fraction of dust-obscured GRBs is likely low, and the afterglow recovery rate for *Swift* bursts may approach unity.

[1] Observatories of the Carnegie Institution of Washington, 813 Santa Barbara Street, Pasadena, CA 91101.
[2] Princeton University Observatory, Peyton Hall, Ivy Lane, Princeton, NJ 08544.
[3] Hubble Fellow.
[4] Division of Physics, Mathematics and Astronomy, 105-24, California Institute of Technology, Pasadena, CA 91125.
[5] Las Campanas Observatory, Carnegie Observatories, Casilla 601, La Serena, Chile.
[6] National Radio Astronomy Observatory, Socorro, NM 87801.
[7] Department of Astronomy and Astrophysics, Pennsylvania State University, 525 Davey Laboratory, University Park, PA 16802.
[8] Department of Astronomy, Yale University, P.O. Box 208101, New Haven, CT 06520-8101.
[9] Institute for Astronomy, University of Hawaii, 2680 Woodlawn Drive, Honolulu, HI 96822.
[10] NASA Goddard Space Flight Center, Greenbelt, MD 20771.
[11] INAF–Osservatorio Astronomico di Brera, Via Bianchi 46, 23807 Merate, Italy.

2. AFTERGLOW IDENTIFICATION AND FOLLOW-UP OF *SWIFT* GAMMA-RAY BURSTS

Properties of the prompt emission (BAT) and X-ray afterglow emission (XRT) for the four *Swift* bursts are summarized in Table 1. Information on our ground-based observations supersedes that given in the GRB Coordinates Network circulars.

2.1. *GRB 041223*

The *Swift* Burst BAT localized this burst on 2004, December 23.5877 UT to a $7'$ radius error circle (Tueller et al. 2004; Markwardt et al. 2004). A series of XRT observations was initiated on December 23.780 UT, and a fading source was detected at R.A. $= 06^{\rm h}40^{\rm m}49\fs2$, decl. $= -37^\circ04'21\farcs5$ (J2000.0) with an uncertainty of about $15''$ radius (Burrows et al. 2004). The spectral energy index was $\beta_x = -1.02 \pm 0.13$, and the temporal decay rate was about $\alpha_x = -1.7 \pm 0.2$ ($F_\nu \propto t^\alpha \nu^\beta$) with a flux of 6.5×10^{-12} ergs cm^{-2} s^{-1} (0.5–10 keV) about 6.2 hr after the burst (Table 1; Burrows et al. 2005). Following our discovery of the optical transient (Berger et al. 2004), the XRT position was revised to (Tagliaferri et al. 2004) R.A. $= 06^{\rm h}40^{\rm m}47\fs4$, decl. $= -37^\circ04'22\farcs3$ (J2000.0), within about $1''$ of the optical afterglow position.

Ground-based observations commenced on December 24.185 UT (14.4 hr after the burst) using the Swope 40 inch (1.02 m) telescope at LCO (Berger et al. 2004). We imaged the entire $7'$ radius BAT error circle in the Gunn *r* band for a total of 20 minutes. The data were bias-subtracted, flat-fielded, and combined using standard IRAF routines. Astrometry was performed relative to the USNO-B catalog using 200 stars in common to the

TABLE 1
PROMPT EMISSION AND X-RAY AFTERGLOW PROPERTIES

GRB (1)	t_0 (UT) (2)	F (ergs cm^{-2}) (3)	t_{90} (s) (4)	α (5)	t_X (s) (6)	F_X (ergs cm^{-2} s^{-1}) (7)	α_X (8)	β_X (9)	References (10)
041223	23.5877	5×10^{-5}	130	1.1	1.63×10^4	6.5×10^{-12}	-1.72 ± 0.20	-1.02 ± 0.13	1, 2, 3
050117a	17.5365	1.7×10^{-5}	220	...	193	1.8×10^{-8}[a]	...	...	4, 5, 6
050124	24.4792	2.1×10^{-6}	4.1	1.5	2.54×10^4	2.2×10^{-12}	...	...	7, 8, 9, 10
050126	26.5001	2.0×10^{-6}	26	1.3	200	2.5×10^{-11}	...	...	11, 12

NOTES.—Prompt emission and X-ray afterglow properties of the four bursts discussed in this paper. Columns: (1) GRB name; (2) burst time; (3) fluence in the 15–350 keV band; (4) burst duration; (5) spectral index; (6) time of X-ray observation; (7) X-ray flux; (8) X-ray temporal decay index; (9) X-ray spectral index.

[a] The X-ray flux of GRB 050117a is dominated by the prompt emission.

REFERENCES.—(1) Tueller et al. 2004; (2) Markwardt et al. 2004; (3) Burrows et al. 2005; (4) Sakamoto et al. 2005; (5) Barthelmy et al. 2005; (6) Hill et al. 2005; (7) Markwardt et al. 2005; (8) Cummings et al. 2005; (9) Pagani et al. 2005; (10) Osborne et al. 2005a; (11) Sato et al. 2005; (12) Kennea et al. 2005.

two frames. The resulting rms positional uncertainty was 0.″15. A stationary source not present in the Digital Sky Survey (DSS) was detected at R.A. = $06^h40^m47^s.323$, decl. = $-37°04'22''.77$ (J2000.0) with a magnitude of $r = 20.99 \pm 0.15$. This position was 7.″5 outside of the initial XRT error circle, but only 1″ from the revised nominal XRT position. A field centered on the position of the afterglow of GRB 041223 is shown in Figure 1, and the observations are summarized in Table 2.

Additional observations with the Swope 40 inch telescope were obtained starting on December 25.15 UT in the r and i bands. A total of 1 hr was obtained in each filter. A comparison of the first and second epochs indicated that the afterglow had faded by 1.2 mag, corresponding to a decay rate of $\alpha_o \approx -1.1$. A similar value was inferred by Burrows et al. (2005) from NIR data. We note that a backward extrapolation of the decay is consistent with the ROTSE-III upper limits obtained at $t = 4.5$ hr (Rykoff 2004).

We subsequently observed the position of the afterglow with the Low Resolution Imager and Spectrograph (LRIS; Oke et al. 1995) mounted on the Keck I 10 m telescope on 2005 January 8.34 UT. We obtained R-band observations for a total of 70 minutes. The data were reduced and analyzed in the manner described above. These observations reveal a faint source at the position of the afterglow with $R = 24.5 \pm 0.3$ mag. An extrapolation of the afterglow flux at $t = 1.56$ days to the epoch of the LRIS observation suggests that this object is most likely the afterglow, although any steepening in the afterglow evolution (e.g., jet break) would mean that the emission is dominated by the host galaxy.

Late-time observations were obtained with the Near Infrared Camera (NIRC; Matthews & Soifer 1994) mounted on the Keck I Telescope in the K_s band on 2005 January 25.33 UT. A total of 62 images of 50 s each were collected. The individual images were dark-subtracted, flat-fielded, and corrected for bad pixels and cosmic rays. We then created object masks, which were used

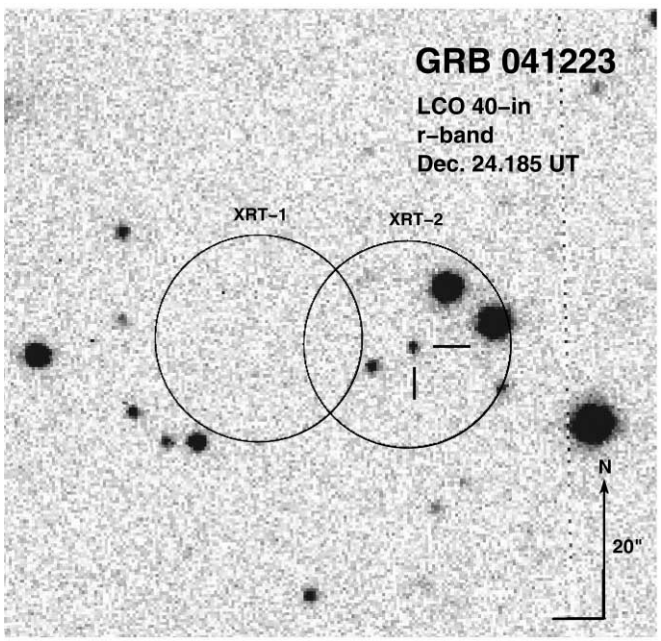

FIG. 1.—Field centered on the position of the optical afterglow of GRB 041223 (*crosshairs*) imaged in the r band with the LCO 40 inch (1.02 m) telescope on December 24.185 UT (14.4 hr after the burst). Also shown are the initial (XRT-1) and revised (XRT-2) 15″ radius error circles from *Swift* XRT.

TABLE 2
GROUND-BASED OPTICAL AND NEAR-INFRARED DATA

Date (UT) (1)	Δt (days) (2)	Telescope[a] (3)	Filter (4)	Magnitude (5)
GRB 041223				
2004 Dec 24.185	0.60	LCO40	r	20.99 ± 0.15
2004 Dec 25.204	1.62	LCO40	r	22.19 ± 0.14
2004 Dec 25.232	1.65	LCO40	i	21.82 ± 0.07
2005 Jan 8.339	15.75	Keck LRIS	R	24.5 ± 0.3
2005 Jan 25.333	32.75	Keck NIRC	K_s	>22.0
GRB 050117a				
2005 Jan 18.146	0.61	P200 WIRC	K_s	>18.5
GRB 050124				
2005 Jan 25.500	1.02	Keck NIRC	K_s	19.66 ± 0.06
2005 Jan 25.486	1.04	Keck NIRC	J	20.90 ± 0.05
2005 Jan 26.472	1.99	Keck NIRC	K_s	20.63 ± 0.18
2005 Jan 26.486	2.01	Keck NIRC	J	22.04 ± 0.17
GRB 050126				
2005 Jan 26.682	0.18	Keck NIRC	K_s	19.45 ± 0.17
2005 Feb 28.526	33.0	P200 WIRC	K_s	20.9 ± 0.3[b]

NOTES.—Ground-based optical and NIR observations of the four bursts discussed in this paper. Columns: (1) UT date of the observation; (2) time since the burst; (3) telescope/instrument; (4) filter; (5) observed magnitude (not corrected for Galactic extinction); limits are 3 σ, and uncertainties are 1 σ.

[a] LCO40 = Swope 40 inch telescope at LCO, and P200 = Hale 200 inch telescope at the Palomar Observatory.

[b] This measurement corresponds to the flux of the host galaxy.

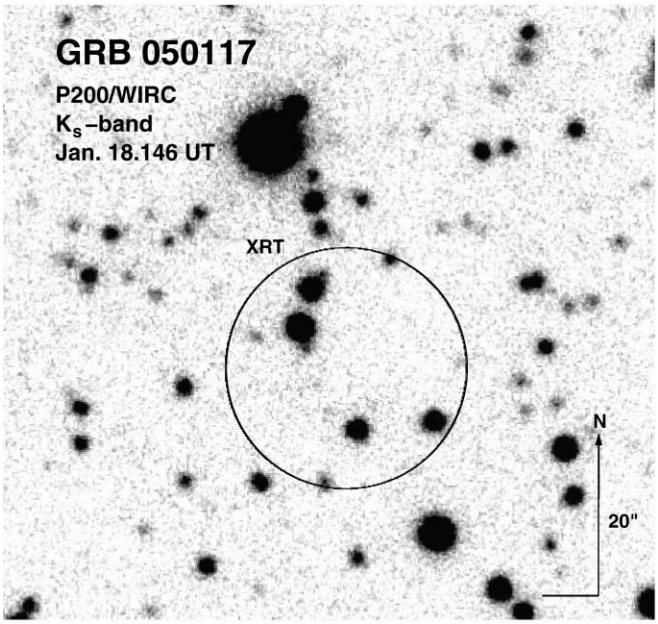

FIG. 2.—Field centered on the XRT position of GRB 050117a imaged in the K_s band with WIRC on the Palomar 200 inch telescope on January 18.146 UT (14.6 hr after the burst). Also shown is the 15″ radius XRT error circle.

to construct improved flat fields for a second round of reduction. The data were finally registered, shifted, and co-added. Photometry was performed relative to three Two Micron All Sky Survey (2MASS) sources in the field, and no object was detected at the position of the afterglow to a 3 σ limit of $K_s = 22.0$ mag.

Finally, we obtained spectroscopic observations using LRIS with a 400 line grating on the red side (dispersion of 1.86 Å pixel^{-1}) and a 600 line grism on the blue side (dispersion of 0.63 Å pixel^{-1}). Two 2400 s exposures were obtained with a 1.″5 slit in 1.″1 seeing. The data were bias-subtracted and flat-fielded using IRAF. Rectification and sky subtraction were performed using the method and software described in Kelson (2003). We detect weak continuum emission, but no obvious emission lines in the range ≈3500–9500 Å.

2.2. *GRB 050117a*

This burst was localized by the BAT on 2005 January 17.5365 UT to a 4′ radius error circle (Sakamoto et al. 2005; Barthelmy et al. 2005). XRT observations revealed a fading source at R.A. = $23^h53^m53^s.0$, decl. = $+65°56'20''$ (J2000.0) with an uncertainty of 15″ radius (Hill et al. 2005). We note that the location of GRB 050117a less than 4° away from the Galactic plane results in large extinction, $E(B-V) = 1.75$ mag (Schlegel et al. 1998), which severely hampered optical searches.

We observed the XRT position of GRB 050117a with the Wide Field Infra-red Camera (WIRC) mounted on the Palomar Hale 200 inch (5.08 m) telescope on January 18.146 UT (14.6 hr after the burst; Fox et al. 2005). A total of 32 minutes were obtained in the K_s band. Several 2MASS and DSS sources were detected within and near the XRT position. A field centered on the XRT error circle of GRB 050117a is shown in Figure 2. At the present no afterglow candidate is identified.

We observed the field with the VLA[12] on 2005 January 19.08 and 24.14 UT (1.54 and 6.60 days after the burst, respectively) at a frequency of 8.46 GHz (Frail 2005; Soderberg & Frail 2005a). No source was detected within the error circle to a 3 σ limit of 98 (January 19.08) and 84 (January 24.14) μJy.

[12] The VLA is operated by the National Radio Astronomy Observatory, a facility of the National Science Foundation operated under cooperative agreement by Associated Universities, Inc.

2.3. *GRB 050124*

This burst was localized by the BAT on 2005 January 24.4792 UT to a 6′ radius error circle (Markwardt et al. 2005; Cummings et al. 2005). An XRT observation was initiated on January 24.607 UT (3.1 hr after the burst), and ground analysis revealed a source at R.A. = $12^h51^m30^s.4$, decl. = $+13°02'39''.0$ (J2000.0), with an uncertainty of 8″ (Pagani et al. 2005; Osborne et al. 2005). The flux of the source was 2×10^{-12} ergs cm^{-2} s^{-1} (2–10 keV; see Table 1).

We observed the XRT 8″ error circle with NIRC in the J and K_s bands starting on January 25.501 (24.5 hr after the burst; Berger & Kulkarni 2005a). A total of 15 minutes were obtained in each band, and the data were reduced in the manner described in § 2.1. Within the XRT error circle we detected a single point source, located at R.A. = $12^h51^m30^s.35$, decl. = $+13°02'41''.3$ (J2000.0). The astrometry was performed relative to an image of the field from the Palomar 60 inch (1.52 m) telescope with an rms positional uncertainty of 0.″2. The NIR afterglow position is only 2.″4 away from the nominal XRT position. Follow-up observations with NIRC on January 26.471 (47.8 hr after the burst) in the J (13.3 minutes) and K_s (14.2 minutes) bands revealed a clear fading of the point source, confirming its identification as the afterglow of GRB 050124 (Berger & Kulkarni 2005b). The brightness of the source was $K_s = 19.66 \pm 0.06$ mag in the first observation, with a decay rate $\alpha_o = -1.45 \pm 0.25$. The observations are summarized in Table 2 and the first epoch NIRC image is shown in Figure 3.

Observations were conducted with the VLA at 4.86 and 8.46 GHz on 2005 January 29.41 UT (4.93 days after the burst;

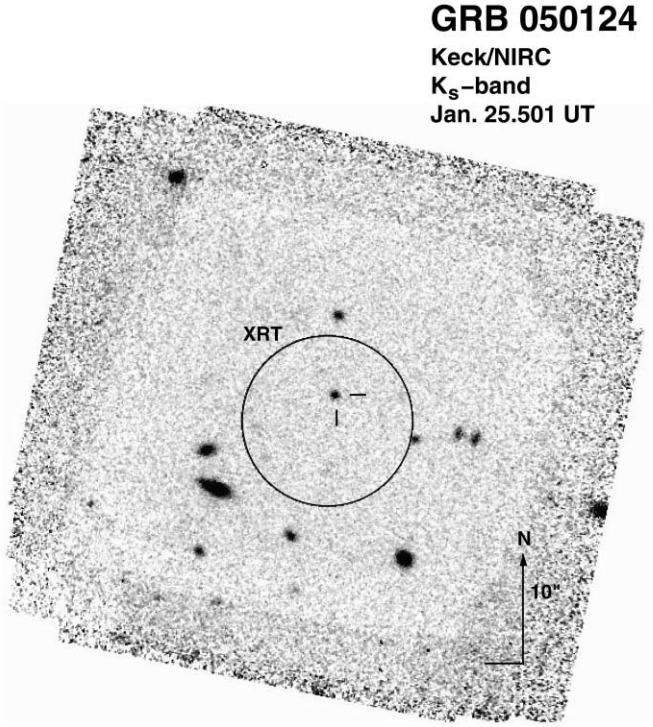

FIG. 3.—Field containing the position of the NIR afterglow of GRB 050124 (*crosshairs*) imaged in the K_s band with NIRC on the Keck I 10 m telescope on January 25.501 UT (24.5 hr after the burst). Also shown is the revised *Swift* XRT 8″ radius error circle.

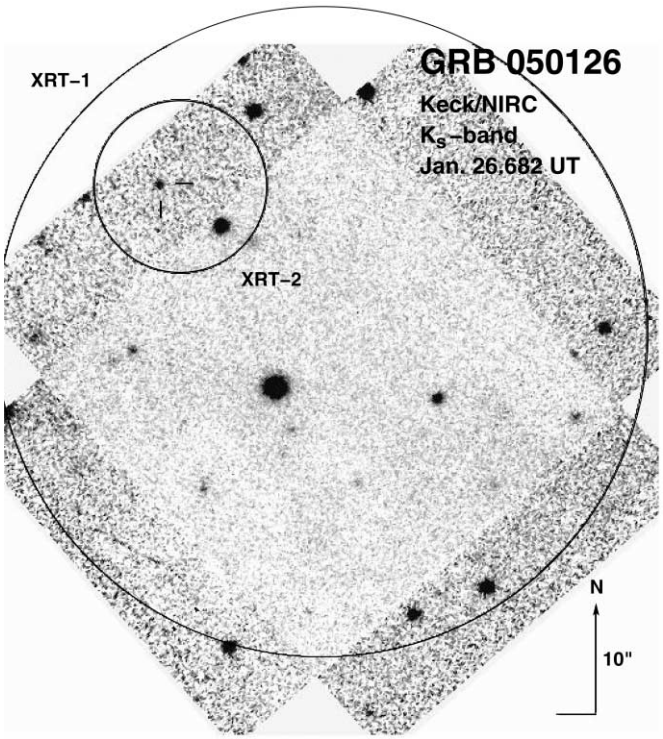

FIG. 4.—Field containing the position of the NIR afterglow of GRB 050126 (*crosshairs*) imaged in the K_s band with NIRC on the Keck I 10 m telescope on January 26.682 UT (4.4 hr after the burst). Also shown are the initial (XRT-1) 30″ radius *Swift* XRT error circle, and the revised (XRT-2) 8″ radius error circle.

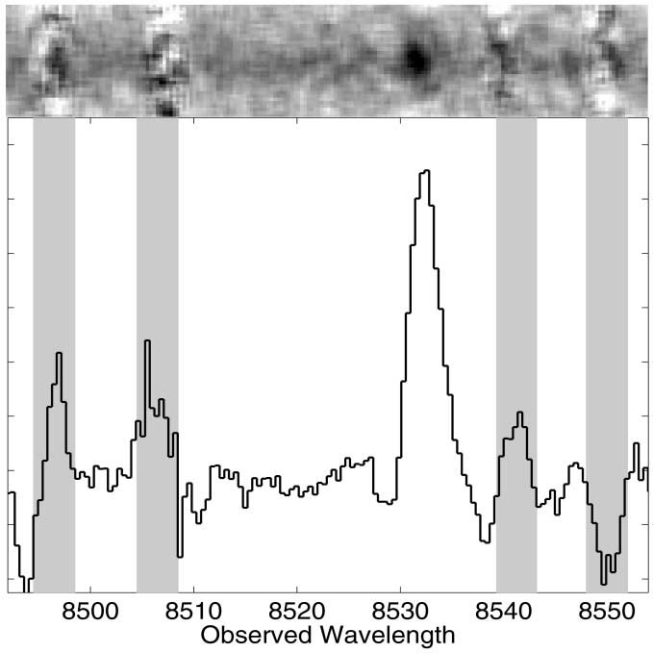

FIG. 5.—Portion of the Keck ESI spectrum of the host galaxy of GRB 050126 centered on the single detected emission line at $\lambda_{obs} = 8532.74 \pm 0.07$ Å. The spectrum has been smoothed with a 7 pixel boxcar. This line is most likely [O II] λ3726.05, indicating a redshift of $z = 1.29002 \pm 0.00002$. The second doublet member is falls on top of the nearby skyline at $\lambda_{obs} \approx 8540$ Å.

Soderberg & Frail 2005b). No source was detected at the position of the NIR afterglow or within the XRT position, to a 3 σ limit of 130 (4.86 GHz) and 100 (8.46 GHz) μJy.

2.4. *GRB 050126*

This burst was localized with the BAT on 2005 January 26.5001 UT to a 4′ radius error circle (Sato et al. 2005). The XRT observation started 129 s after the burst and revealed a source that was localized to a 30″ error circle (Kennea et al. 2005). Ground analysis based on data from four orbits resulted in a refined position of 8″ accuracy (Campana et al. 2005) centered on R.A. = $18^h32^m27\overset{s}{.}0$, decl. = $+42^\circ22'13\overset{''}{.}5$ (J2000.0).

We observed the XRT 30″ error circle with NIRC in the K_s band starting on 2005 January 26.682 UT (4.4 hr after the burst; Berger & Kulkarni 2005c; Berger 2005) for a total of 8.3 minutes. The data were reduced in the manner outlined above, and astrometry was performed relative to the DSS using six stars in common between the two images. The resulting rms positional uncertainty was 0.12. Within the revised XRT error circle we detect one object not visible in the DSS at R.A. = $18^h32^m27\overset{s}{.}18$, decl. = $+42^\circ22'13\overset{''}{.}6$ (J2000.0). This position is only 2.″0 away from the nominal XRT position. The source has $K_s = 19.45 \pm 0.17$ mag. The NIRC image is shown in Figure 4. Observations of the afterglow candidate on 2005, February 28.53 UT using the WIRC camera on the Palomar 200 inch telescope reveal that the afterglow has faded by at least 1.36 mag, indicating that $\alpha_o < -0.3$. A faint source is detected at the same position which we consider to be the host galaxy. We note that the afterglow of GRB 050126 is the faintest detected to date (see Fig. 6 and Klose et al. 2003).

We obtained spectra of the host galaxy using the Echelle Spectrograph and Imager (ESI) mounted on the Keck II 10 m telescope on 2005 March 6 and 7 UT. A total of four 2700 s exposures were obtained with a 1″ slit in 0.″9 seeing. The data were bias-subtracted and flat-fielded using IRAF. Rectification and sky subtraction were performed using the method and software described in Kelson (2003). Wavelength calibration was performed using a combination of Cu/Ar and Xe/Hg/Ne arc lamps, and air-to-vacuum and heliocentric corrections were applied. We detect a single emission at an observed wavelength of 8532.74 ± 0.07 Å, which we interpret as [O II] λ3726.05 at a redshift of $z = 1.29002 \pm 0.00002$. The second doublet member is masked by a nearby skyline (Fig. 5). Given a fluence of 2×10^{-6} ergs cm^{-2} (Table 1), we conclude that the isotropic-equivalent gamma-ray energy of the burst was 8.7×10^{51} ergs.

We observed the position of GRB 050126 with the VLA at 8.46 GHz on 2005 January 26.67 and 28.59 UT (4.1 hr and 2.09 days after the burst, respectively). No object was detected at the position of the NIR candidate or within the revised XRT error circle to a limit of about 100 μJy (Frail & Soderbergs 2005).

3. AFTERGLOW PROPERTIES

We now provide a simple analysis of the afterglow emission from the individual bursts. For GRB 041223 we combine the data presented in this paper with measurements in the *J* and *K* bands from Burrows et al. (2005). Correcting for Galactic extinction ($A_R = 0.32, A_I = 0.23, A_J = 0.11$, and $A_K = 0.04$ mag; Schlegel et al. 1998), we find that the best-fit spectral index using all the available optical/NIR observations is $\beta_o = -0.6 \pm 0.1$, while the best-fit temporal decay rate is $\alpha_o = -1.1 \pm 0.1$. In the absence of significant extinction within the host galaxy, we can use these values, along with the synchrotron closure relations (e.g., Berger et al. 2002), to determine the value of the electron distribution power-law index, p [$N(\gamma) \propto \gamma^{-p}$], the geometry of the circumburst environment (interstellar medium [ISM] or wind), and the location of the synchrotron cooling frequency

relative to the optical/NIR band. Three possibilities exist, namely, $\alpha - 3\beta/2 = 0$ ($\mathrm{ISM_{blue}}$), $\alpha - 3\beta/2 - 1/2 = 0$ ($\mathrm{ISM_{red}}$ and $\mathrm{wind_{red}}$), and $\alpha - 3\beta/2 + 1/2 = 0$ ($\mathrm{wind_{blue}}$); the subscript designates whether the cooling frequency is blueward or redward of the optical/NIR band. The $\mathrm{ISM_{blue}}$ closure relation provides the best result, -0.2 ± 0.25, indicating that $p = 2.2 \pm 0.2$, and the cooling frequency is located blueward of the optical/NIR band. This conclusion is supported by the X-ray spectral index, $\beta_{\mathrm{X}} = -1.0 \pm 0.1$, which implies $p = 2.0 \pm 0.2$ if ν_c is located redward of the X-ray band.

A comparison of the optical/NIR flux and the X-ray flux, extrapolated to a common time of 19.6 hr using $\alpha_{\mathrm{X}} = -1.7$, indicates that the spectral index between the two bands is $\beta_{\mathrm{ox}} \approx -0.65$. Taken in conjunction with the individual optical/NIR and X-ray spectral indices, this indicates that the cooling frequency is $\nu_c \approx 1.1 \times 10^{17}$ Hz or about 0.45 keV. We note, however, that in the context of this model, the X-ray temporal decay is expected to be $\alpha_{\mathrm{X}} = -1.1 \pm 0.1$, which is about 2.7 σ away from the measured value, $\alpha_{\mathrm{X}} = -1.7 \pm 0.2$. The steeper decay may be due to a contribution from inverse Compton emission (Sari & Esin 2001). We note that Burrows et al. (2005) suggest that the optical/NIR and X-ray afterglows are dominated by two different physical components.

We perform a similar analysis for GRB 050124. Based on the pair of J- and K_s-band observations taken on the first and second nights after the burst, we find a spectral index, $\beta_o = -0.4 \pm 0.2$, and a temporal decay index $\alpha_o = -1.45 \pm 0.25$. These values satisfy the closure relation for the $\mathrm{wind_{blue}}$ case, -0.35 ± 0.55, indicating that $p = 2.1 \pm 0.3$ and the cooling frequency is located blueward of the NIR bands. A comparison of the X-ray flux at 7.1 hr after the burst to the NIR flux, extrapolated to the epoch of the X-ray observations using the measured value of α, indicates an optical/X-ray spectral index, $\beta_{\mathrm{ox}} \approx -0.5$, in good agreement with the optical/NIR spectral index. This suggests that the cooling break is most likely located near the X-ray band.

Finally, for GRB 050126 we simply note that the decay rate of the NIR afterglow is steeper than $\alpha_o \approx -0.3$. Both the NIR and X-ray afterglows are fainter than any other afterglow detected to date. For the purpose of this comparison we extrapolate the NIR flux to the optical R band using a typical spectral index of -0.6, and the X-ray flux from 200 s to 10 hr using $\alpha_{\mathrm{X}} \approx -1.3$, which is typical for X-ray afterglows (Berger et al. 2003).

4. DISCUSSION AND CONCLUSIONS

One of the main promises of *Swift* is rapid localization and follow-up with the XRT and UVOT. The X-ray fluxes from XRT (Burrows et al. 2005; J. E. Hill et al., in preparation; J. P. Osborne et al., in preparation; G. Tagliaferri et al. 2005, in preparation) are summarized in § 2 and Table 1. In Figure 6 we plot the X-ray fluxes normalized to 10 hr after the burst in comparison to the sample of Berger et al. (2003). We find that three of the four XRT afterglows are typical of the general population, but the X-ray afterglow of GRB 050126 is the faintest detected to date (when normalized to 10 hr), and it was only detected thanks to the rapid response of the XRT. The fluxes were extrapolated to the common epoch using the measured temporal decay index or the typical $F_\nu \propto t^{-1.3}$ (Berger et al. 2003). We note that the X-ray flux for GRB 050117a is dominated by the prompt emission and should be considered an upper limit.

Similarly, we plot the R-band magnitudes of the *Swift* afterglows, measured directly or extrapolated from the NIR (using the measured spectral indices or a typical $F_\nu \propto \nu^{-0.6}$), in comparison to a compilation of optical light curves collected in the past 7 yr. We find that the afterglows are fainter than about 70% of the population on a similar timescale (Fig. 6). In particular, the afterglow of GRB 050126 is the faintest detected to date. We note that the subsequent detection of the NIR afterglow of GRB 050215b reveals an equally faint afterglow (Tanvir et al. 2005). The afterglow detections are due to the accurate positions available from the XRT, which allowed us to both identify the afterglows more readily and search the error circles in the NIR with a large aperture telescope. We note that the faintness of the optical afterglows may also explain the nondetections in the radio.

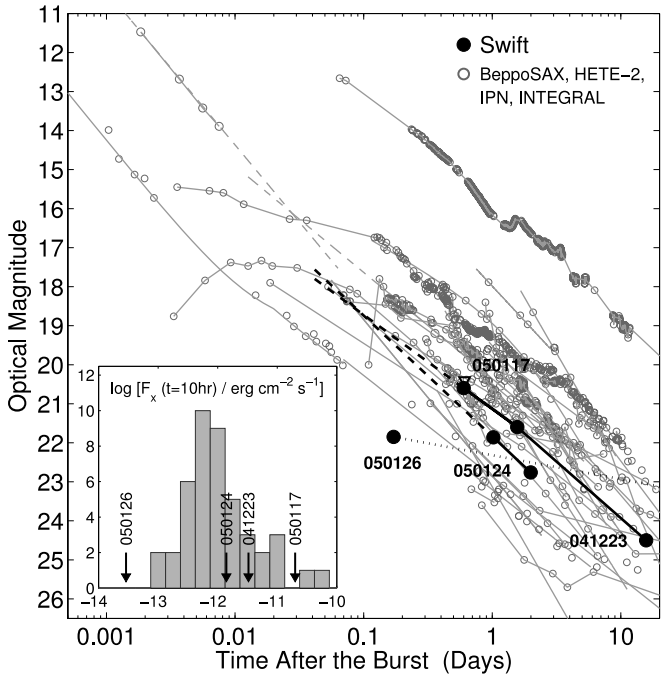

FIG. 6.—Optical light curves of the *Swift* bursts discussed in this paper (and upper limit on GRB 050117a) compared to the sample of afterglows detected and studied in the past 7 yr. We transformed the NIR flux of GRB 050124 to the R band using the measured spectral index, and that of GRB 050126 assuming a typical index of $\beta = -0.6$. The dotted line indicates the minimum decay rate for GRB 050126 ($\alpha_o \approx -0.3$) given the nondetection in the second epoch (Table 2). The *Swift* optical/NIR afterglows are fainter than about 70% of the known afterglow population. Their detection was due to the small error circles from XRT and searches with large telescopes. The inset shows the distribution of X-ray fluxes at $t = 10$ hr after the burst for the XRT bursts (using measured temporal decay indices or assuming the typical $\alpha_{\mathrm{X}} = -1.3$) compared to the sample of Berger et al. (2003). Three of the four afterglows are typical of the general population, but the afterglow of GRB 050126 is the faintest detected to date, in agreement with the faintness of the NIR afterglow. We note that the X-ray emission for GRB 050117a is contaminated by the prompt emission and should be considered as an upper limit.

Several conclusions can already be drawn from this early work. First, nearly every XRT localization has resulted in the identification of an optical or NIR afterglow; the single exception (GRB 050117a) is likely due to large Galactic extinction. The optical/NIR afterglow recovery rate for XRT (9/13 as of GRB 050319) and the *High Energy Transient Explorer 2* SXC[13] (11/13) is about 80%. The brightness of the XRT+SXC sample normalized to $t = 12$ hr compared to all other optical afterglows is shown in Figure 7. The afterglows of the XRT bursts appear to be fainter than about 70% of all afterglows detected prior to

[13] We use only the SXC bursts for this purpose since these have accurate positions ($\lesssim 2'$) and rapid localizations ($\sim$hours) and are therefore not influenced by observational difficulties.

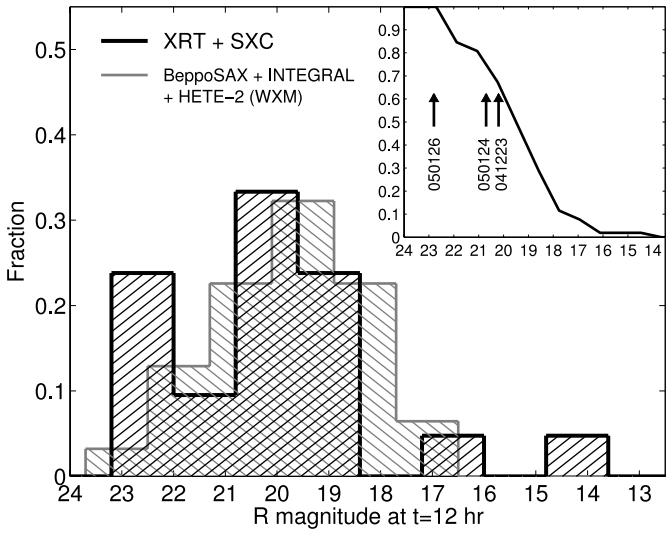

FIG. 7.—Distribution of *R*-band magnitudes normalized to 12 hr after the burst for the XRT+SXC sample (*black*; 21 afterglows) compared to all other optical afterglows (*gray*; 31 afterglows). The afterglow detection rate for the XRT+SXC sample is about 80%, suggesting that the fraction of dust-obscured ("dark") GRBs is small. The inset shows the cumulative distribution for all afterglows discovered prior to *Swift* along with the three afterglows discussed in this paper. The *Swift* XRT bursts are fainter than about 70% of all afterglows localized to date. In the past, these may have been designated as dark.

Swift, suggesting that past nondetections were mainly the result of large error regions and/or shallow searches. This indicates that the fraction of "dark" (dust-obscured) GRBs is low, although we note that two of the XRT bursts were localized in the NIR and may still be dust-obscured. If this trend persists then this bodes well for identification of high redshift afterglows using the Lyman break technique, since the main contaminant is dust-obscured bursts.

Second, in the three cases in which an optical/NIR afterglow was detected, the offset relative to the nominal XRT position has been $\lesssim 2''$, much less than the size of the error circles. This suggests that in the near future the XRT will be capable of providing $\sim 2''$ positions. This will significantly reduce the delay from localization to identification of the optical/NIR afterglow in cases when a UVOT subarcsecond position is not available.

We end by noting that the faintness of the optical/NIR afterglows studied in this paper ($R \approx 18$ mag at $\Delta t = 1$ hr; Figs. 6 and 7) may make it difficult for small robotic telescopes to provide long-term follow-up of *Swift* bursts. However, larger telescopes, while somewhat slower to respond, will allow both long-term follow-up and detection of the faintest afterglows, particularly in the NIR.

We thank the staff at the Las Campanas Observatory, the Palomar Observatory, the Keck Observatory, and the Very Large Array. We also thank Mario Hamuy for generous use of his observing time and Dan Kelson for help with his sky background subtraction software. E. B. is supported by NASA through Hubble Fellowship grant HST-01171.01, awarded by the Space Telescope Science Institute, which is operated by AURA, Inc., for NASA under contract NAS 5-26555. Additional support was provided by NSF and NASA grants. A. G. acknowledges support by NASA through Hubble Fellowship grant HST-HF-01158.01-A, awarded by STScI, which is operated by AURA, Inc., for NASA, under contract NAS 5-26555.

REFERENCES

Barthelmy, S., et al. 2005, GCN Circ. 2962, http://gcn.gsfc.nasa.gov/gcn/gcn3/2962.gcn3
Berger, E. 2005, GCN Circ. 2997, http://gcn.gsfc.nasa.gov/gcn/gcn3/2997.gcn3
Berger, E., Krzeminski, W., & Hamuy, M. 2004, GCN Circ. 2902, http://gcn.gsfc.nasa.gov/gcn/gcn3/2902.gcn3
Berger, E., & Kulkarni, S. R. 2005a, GCN Circ. 2978, http://gcn.gsfc.nasa.gov/gcn/gcn3/2978.gcn3
———. 2005b, GCN Circ. 2983, http://gcn.gsfc.nasa.gov/gcn/gcn3/2983.gcn3
———. 2005c, GCN Circ. 2985, http://gcn.gsfc.nasa.gov/gcn/gcn3/2985.gcn3
Berger, E., Kulkarni, S. R., & Frail, D. A. 2003, ApJ, 590, 379
Berger, E., et al. 2002, ApJ, 581, 981
Burrows, D. N., et al. 2004, GCN Circ. 2901, http://gcn.gsfc.nasa.gov/gcn/gcn3/2901.gcn3
———. 2005, ApJ, 622, L85
Campana, S., et al. 2005, GCN Circ. 2996, http://gcn.gsfc.nasa.gov/gcn/gcn3/2996.gcn3
Cummings, J., et al. 2005, GCN Circ. 2973, http://gcn.gsfc.nasa.gov/gcn/gcn3/2973.gcn3
Fox, D. B., Cenko, S. B., & Murphy, E. 2005, GCN Circ. 2960, http://gcn.gsfc.nasa.gov/gcn/gcn3/2960.gcn3
Frail, D. A. 2005, GCN Circ. 2963, http://gcn.gsfc.nasa.gov/gcn/gcn3/2963.gcn3
Frail, D. A., & Soderberg, A. M. 2005, GCN Circ. 2993, http://gcn.gsfc.nasa.gov/gcn/gcn3/2993.gcn3
Gehrels, N., et al. 2004, ApJ, 611, 1005
Hill, J. E., et al. 2005, GCN Circ. 2955, http://gcn.gsfc.nasa.gov/gcn/gcn3/2955.gcn3
Kelson, D. D. 2003, PASP, 115, 688
Kennea, J. A., et al. 2005, GCN Circ. 2984, http://gcn.gsfc.nasa.gov/gcn/gcn3/2984.gcn3
Klose, S., et al. 2003, ApJ, 592, 1025
Markwardt, C., et al. 2004, GCN Circ. 2909, 1
———. 2005, GCN Circ. 2972, http://gcn.gsfc.nasa.gov/gcn/gcn3/2972.gcn3
Matthews, K., & Soifer, B. T. 1994, in Infrared Astronomy with Arrays: The Next Generation (Dordrecht: Kluwer), 239
Oke, J. B., et al. 1995, PASP, 107, 375
Osborne, J. P., et al. 2005, GCN Circ. 2975, http://gcn.gsfc.nasa.gov/gcn/gcn3/2975.gcn3
Pagani, C., et al. 2005, GCN Circ. 2974, http://gcn.gsfc.nasa.gov/gcn/gcn3/2974.gcn3
Rykoff, E. 2004, GCN Circ. 2899, http://gcn.gsfc.nasa.gov/gcn/gcn3/2899.gcn3
Sakamoto, T., et al. 2005, GCN Circ. 2952, http://gcn.gsfc.nasa.gov/gcn/gcn3/2952.gcn3
Sari, R., & Esin, A. A. 2001, ApJ, 548, 787
Sato, G., et al. 2005, GCN Circ. 2987, 1
Schlegel, D. J., Finkbeiner, D. P., & Davis, M. 1998, ApJ, 500, 525
Soderberg, A. M., & Frail, D. A. 2005a, GCN Circ. 2980, http://gcn.gsfc.nasa.gov/gcn/gcn3/2980.gcn3
———. 2005b, GCN Circ. 3000, http://gcn.gsfc.nasa.gov/gcn/gcn3/3000.gcn3
Tagliaferri, G., et al. 2004, GCN Circ. 2910, http://gcn.gsfc.nasa.gov/gcn/gcn3/2910.gcn3
Tanvir, G., et al. 2005, GCN Circ. 3031, http://gcn.gsfc.nasa.gov/gcn/gcn3/3031.gcn3
Tueller, J., et al. 2004, GCN Circ. 2898, http://gcn.gsfc.nasa.gov/gcn/gcn3/2898.gcn3